Chirped Microwave Pulse Generation Using an Integrated SiP Bragg Grating in a Sagnac Loop

Junjia Wang, *Student Member, IEEE*, Reza Ashrafi, *Member, IEEE*, Martin Rochette, *Senior Member, IEEE*, and Lawrence R. Chen, *Senior Member, IEEE*

***Abstract*— We demonstrate an integrated spectral shaper based on a Sagnac loop incorporating a chirped Bragg grating in silicon photonics for the photonic generation of chirped microwave pulses. The technique is based on optical spectral shaping combined with linear frequency-to-time mapping. By tuning the central wavelength of the input optical pulse, we obtain chirped microwave pulses with central frequencies ranging from ∼10 GHz to ∼30 GHz and an RF chirp rate of ∼20 GHz/ns with both positive and negative signs.**

***Index Terms*— Silicon photonics, microwave photonics, optical spectral shaping, chirped microwave pulse generation, integrated waveguide Bragg gratings, frequency-to-time mapping.**

I. Introduction

HIGH-FREQUENCY microwave waveform generation with large time-bandwidth product (TBP) has attracted considerable attention for a wide range of applications, including radar, telecommunications, imaging, and sensing systems [1], [2]. For example, chirped or phase–modulated microwave pulses are used to increase range resolution and detection distance in radar systems [1]. Chirped microwave pulses can be generated in the electrical domain using a voltage controlled oscillator. The major difficulty associated with the use of an electronic oscillator is that the central frequency and the bandwidth of the generated pulses are limited, with typically reported signal content below ∼5 GHz [3]. However, for the next generation of radar and medical imaging systems, microwave pulses with central frequencies up to 10s or even 100s of GHz are required [1]. Recently an important body of research towards this aim has focused on using photonic techniques in which high-frequency microwave signals are generated/processed in the optical domain using photonics components. This approach benefits from the extremely large bandwidth available in the optical domain, and several interesting photonics-based techniques have been demonstrated for high-frequency microwave waveform generation [4]–[11]. The main demonstrated approaches for photonic generation of microwave pulses include techniques based on spatial-domain optical filtering [4], [5], linearly chirped optical pulse interference [6], heterodyne beating between a pre-chirped optical pulse and a continuous wave light [7], and optical spectral shaping followed by linear or nonlinear frequency-to-time mapping (FTM) in a dispersive element [8]–[10]. Integrated silicon photonic (SiP) solutions are attracting considerable attention [11]–[13] to implement microwave photonic signal processing systems to address issues such as compactness, manufacturability, stability, and reliability.

Manuscript received March 12, 2015; revised May 11, 2015; accepted June 6, 2015. Date of publication June 10, 2015; date of current version August 5, 2015. This work was supported in part by the Natural Sciences and Engineering Research Council of Canada, in part by the Integrated Silicon Photonic Spectral Shapers through the University of Washington Nanofabrication Facility, and in part by the National Science Foundation National Nanotechnology Infrastructure Network.

The authors are with the Department of Electrical and Computer Engineering, McGill University, Montréal, QC H3A 0E9, Canada (e-mail: junjia.wang@mail.mcgill.ca; reza.ashrafi@mail.mcgill.ca; martin.rochette@mcgill.ca; lawrence.chen@mcgill.ca).

Color versions of one or more of the figures in this letter are available online at http://ieeexplore.ieee.org.

Digital Object Identifier 10.1109/LPT.2015.2444275

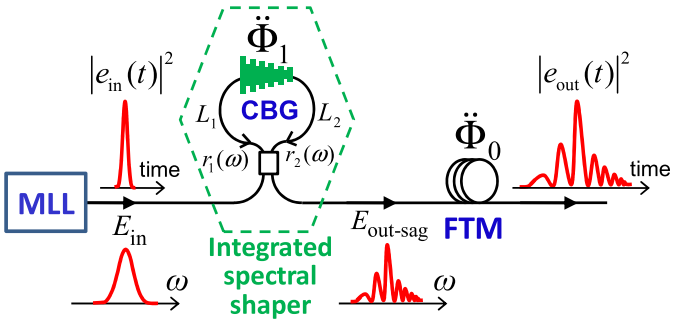

Fig. 1. Schematic of the implemented system for chirped microwave pulse generation.

In this letter, we demonstrate an integrated optical spectral shaper in SiP for the photonic generation of chirped microwave pulses. The approach is based on optical spectral pulse shaping followed by linear FTM. The general concept is similar to the fiber-optic technique presented in [9]; however, notable differences include our approach for tuning the central frequency and chirp rate of the generated microwave pulses. In the original implementation of the idea [9], the tunability of the central frequency and chirp sign of the generated microwave pulse was achieved through tuning the time-delay in the fiber-based Sagnac loop. However tunable time-delay implementation in an integrated format is a challenging issue. In this regard, we have proposed a new technique of achieving the central frequency and chirp sign tunability based on tuning the input pulse central wavelength. We also present a new simplified theoretical derivation for the main figure of merit parameters of the waveform generation process.

II. Operation Principle

Fig. 1 shows a schematic of the microwave pulse generation system. The system comprises a cascade of two linear optical processes: spectral shaping and FTM. Briefly, the spectrum of

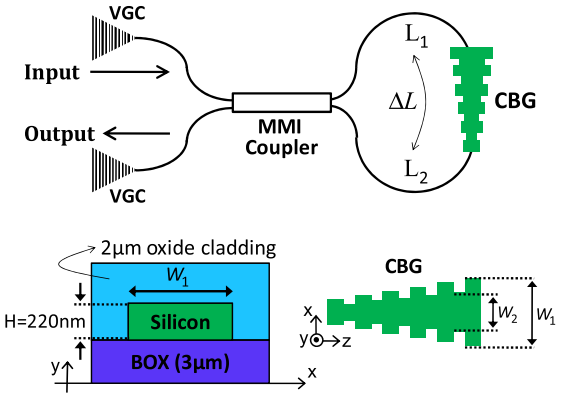

Fig. 2. Schematic of the fabricated integrated silicon photonic spectral shaper for chirped microwave pulse generation.

an input optical pulse is tailored in the spectral shaping device; this spectral profile is then mapped into the time-domain after the FTM process [14]. The FTM process is carried out by propagation in a length of dispersive fiber. The spectral shaper is based on an integrated Sagnac loop incorporating a chirped Bragg grating (CBG), as illustrated in Fig. 2.

The CBG is designed to achieve the maximum reflection peak and negligible transmission over its response bandwidth denoted BW_{opt}. The complex spectral amplitude of the pulses reflected back to the multi-mode interference (MMI) coupler, within the frequency bandwidth of $|\omega| \leq (2\pi \cdot BW_{\text{opt}})/2$, by subtracting the common propagation group delay (and leaving only the time-delay mismatch, τ), can be written as

$$r_1(\omega) \propto E_{\text{in}}(\omega) \cdot \exp\left[-j\left(+\ddot{\Phi}_1/2\right)\omega^2 - j\tau\omega\right], \quad (1)$$

$$r_2(\omega) \propto E_{\text{in}}(\omega) \cdot \exp\left[-j\left(-\ddot{\Phi}_1/2\right)\omega^2\right], \quad (2)$$

where $r_1(\omega)$ and $r_2(\omega)$ are the reflected pulses from the two arms of the Sagnac loop with lengths L_1 and L_2, respectively (see Fig. 1), ω is the relative angular frequency with respect to the central angular frequency ω_0, corresponding to the central Bragg wavelength λ_0 of the CBG, i.e., $\omega_0 = 2\pi c/\lambda_0$, where c is the light speed in vacuum. $E_{\text{in}}(\omega)$ is the input pulse complex spectral amplitude and as it will be specified in what follows, it is not necessarily centered around $\omega = 0$. τ is the time-delay mismatch corresponding to the length mismatch $\Delta L = L_1 - L_2$ in the two arms of the Sagnac loop: $\tau = (2\Delta L \cdot n_{\text{g}})/c$, where n_{g} is the average group index of the silicon waveguide. $\ddot{\Phi}_1$ [s^2] is the second-order dispersion of the CBG which is related to the chirp parameter C_{CBG} [nm/mm] of the CBG by [15]:

$$\ddot{\Phi}_1 = 2\pi / \left(\omega_0^2 \cdot C_{\text{CBG}}\right). \quad (3)$$

Note that Eq. (3) is obtained when assuming a fixed CBG length L_{CBG}. The signal power $|E_{\text{out-sag}}(\omega)|^2$ at the output of the spectral shaper can be expressed as:

$$\left|E_{\text{out-sag}}(\omega)\right|^2 \propto |r_1(\omega) + r_2(\omega)|^2 \propto |E_{\text{in}}(\omega)|^2 \cdot \left\{1 + \cos\left(\tau\omega + \ddot{\Phi}_1\omega^2\right)\right\}. \quad (4)$$

Therefore the power frequency transfer function $P(\omega)$ and the free spectral range (FSR) of the spectral shaper are:

$$P(\omega) = \left|E_{\text{out-sag}}(\omega)\right|^2 / |E_{\text{in}}(\omega)|^2 \propto 1 + \cos\left(\tau\omega + \ddot{\Phi}_1\omega^2\right), \quad (5)$$

$$FSR(\omega) \cong 2\pi / \left|\tau + \ddot{\Phi}_1\omega\right|. \quad (6)$$

The output signal from the spectral shaper is passed through the FTM process in a length of dispersive fiber with a total second-order dispersion $\ddot{\Phi}_0$. Consider the center of the input pulse spectrum $E_{\text{in}}(\omega)$ to be tuned around $\omega = 0 - \delta\omega$, where $\delta\omega$ is the angular frequency detuning with respect to ω_0. The wavelength detuning $\delta\lambda$ is also defined as $\delta\lambda = (2\pi c/\omega_0^2) \cdot \delta\omega$. The time-domain profile $|e_{\text{out}}(t)|^2$, the central microwave frequency f_{C} [Hz] and the linear chirp rate C_{RF} [Hz/s] of the generated microwave pulse can be expressed as (see Refs [9], [10] for basic definitions):

$$|e_{\text{out}}(t)|^2 \propto |a(t)|^2 \cdot \left[1 + \cos\left(\frac{\tau + 2\ddot{\Phi}_1 \cdot \delta\omega}{\ddot{\Phi}_0}t + \frac{\ddot{\Phi}_1}{\ddot{\Phi}_0^2}t^2\right)\right], \quad (7)$$

$$f_{\text{C}} = \frac{1}{2\pi}\left|\frac{\tau + 2\ddot{\Phi}_1 \cdot \delta\omega}{\ddot{\Phi}_0}\right|, \quad (8)$$

$$C_{\text{RF}} = \frac{1}{2\pi}\text{sgn}\left(\frac{\tau + 2\ddot{\Phi}_1 \cdot \delta\omega}{\ddot{\Phi}_0}\right) \cdot \frac{2\ddot{\Phi}_1}{\ddot{\Phi}_0^2}, \quad (9)$$

where $\text{sgn}(x) = 1$ for $x > 0$, 0 for $x = 0$, and -1 for $x < 0$. Also $|a(t)|^2$ is the temporal power envelope of the generated microwave pulse which is centered around $t = 0$. Note that there is a constant phase term in Eq. 7 which has been neglected, since it does not play any role in our waveform generation application. As it can be seen in Eq. (8), for a given FTM dispersion $\ddot{\Phi}_0$, the central RF frequency of the generated chirped microwave pulse, is determined by the absolute value of the length mismatch ΔL (or its corresponding time-delay mismatch τ) and the center of the input pulse spectrum defined by $\delta\omega$. Also for a given FTM dispersion, the RF chirp rate of the generated microwave pulse only depends on the second-order dispersion value $\ddot{\Phi}_1$ provided by the CBG, see Eq. (9). The TBP of the generated chirped microwave pulse is defined as the product of the temporal duration and the bandwidth of the generated microwave pulse. The TBP in our approach (similar to Ref. [9]) is independent of the FTM dispersion value and it only depends on the frequency response features of the employed spectral shaper. In particular, the TBP can be expressed as a function of two figure of merit parameters of the employed CBG: (i) the optical response bandwidth (BW_{opt}) and (ii) the second-order dispersion $\ddot{\Phi}_1$of the CBG. Let us assume the input pulse bandwidth is as large as BW_{opt} and is tuned to be centered on $\omega = 0$ (i.e., $\delta\omega = 0$). To exploit the maximum TBP provided by the CBG, the time-delay mismatch in the Sagnac loop should be larger than a minimum value of

$$\tau_{\min} \cong \pi \left|\ddot{\Phi}_1\right| \cdot BW_{\text{opt}}. \quad (10)$$

By having $|\tau| > \tau_{\min}$, the generated chirped microwave pulse can achieve a maximum TBP of

$$TBP_{\max} = 2\pi \left|\ddot{\Phi}_1\right| \cdot BW_{\text{opt}}^2. \quad (11)$$

Note that by having $|\tau| > \tau_{\min}$ the frequency response of the spectral shaper will exhibit a purely (monotonic) decreasing/increasing modulation period over the whole bandwidth BW_{opt} of the CBG. This will result into only having a single RF chirp sign (positive or negative) for the generated chirped microwave pulse. However, in many applications, the ability to change the sign of RF chirp is desirable. In this regard, for the fabricated integrated spectral shaper, we have chosen a time-delay mismatch $|\tau|$ to be smaller than $\tau_{\min}$. In this manner, we achieve tunability of the RF chirp sign along with tunability of the RF central frequency by tuning central wavelength of the input optical pulse. Note that for $\tau = 0$, the spectral response is symmetric around λ_0 and the FSR decreases with increased wavelength detuning (from λ_0). By increasing the length mismatch ΔL and correspondingly increasing $|\tau|$, the spectral response is no longer symmetric around λ_0 and in this manner we can control the variation in FSR.

An important practical consideration concerns the fact that to increase the chirp in the FSR of the spectral shaper and correspondingly to increase the chirp rate (C_{RF}) of the generated microwave pulse, the second-order dispersion coefficient $\ddot{\Phi}_1$ provided by the CBG should be increased, see Eq. (9). According to Eq. (3), this requires the grating chirp rate (C_{CBG}) of the CBG to be decreased. However, in a CBG with a fixed length L_{CBG}, decreasing the grating chirp rate will decrease the device response bandwidth BW_{opt} [15]. By considering a practical limited length for an integrated CBG, this reveals a trade-off between the achievable second-order dispersion $\ddot{\Phi}_1$ and the response bandwidth BW_{opt} of the device. Note that the maximum temporal duration of the generated chirped microwave pulse is ultimately determined by the bandwidth BW_{opt} of the CBG, i.e., by assuming the input pulse bandwidth to be as large as BW_{opt}.

III. Experiments

A. Device Design and Experimental Details

The integrated spectral shaper design parameters are as follows, see Fig. 2. The Si waveguide thickness is H = 220 nm on top of a 3 μm buried oxide (BOX) layer on a Si substrate and it is covered by a 2 μm index-matched oxide cladding layer. The waveguide width is 500 nm and vertical grating couplers (VGCs), which couple light into and out of the chip, are optimized for TE mode operation. The width of the MMI coupler is 6 μm with a length of 127 μm; the splitting ratio is designed to be 50:50. L_1 and L_2 represent the lengths of the waveguides between the output of the MMI coupler to the two ports of the CBG device. Two spectral shapers with different length mismatch (i.e., $\Delta L = L_1 - L_2$) of 100μm and 400μm have been fabricated. The CBG has a length of 3.2 mm and is based on sidewall corrugations with a corrugation depth of $(W_1 - W_2)/2 = 10$ nm, and a grating period of 320 nm, as illustrated in Fig. 2. To realize a chirped grating, the waveguide width W_1 is increased from 500 nm to 510 nm over the 3.2 mm length of the CBG. On the wider side of the CBG, a 10 μm long taper connects the CBG waveguide width of 510 nm to the waveguide width of 500 nm, to prevent unwanted reflections. The grating chirp is estimated to be $C_{\text{CBG}} \sim 0.26$ nm/mm.

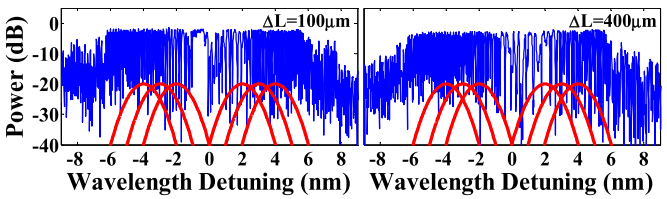

Fig. 3. The measured power frequency responses of the two fabricated spectral shapers with ΔL= 100μm and 400μm (blue curves). The normalized input pulse spectra has also been shown (red curves).

In our experiments, the input is a Gaussian-like optical pulse with a full width at half maximum (FWHM) bandwidth of 1.5 nm which is generated using a passively mode-locked fiber laser (MLL) (CALMAR Inc., cascaded with a tunable filter) with a repetition rate of 20 MHz. The dispersive fiber employed to perform the FTM process is a ~24 km spool of standard single-mode fiber (SMF-28e, Corning Inc.); the corresponding second-order dispersion for the FTM process is $\ddot{\Phi}_0 = 528$ ps^2.

B. Results

The measured power frequency responses of the two fabricated spectral shapers with $\Delta L = 100$ μm and 400 μm are shown in Fig. 3. The measured central Bragg wavelengths of the devices are $\lambda_0 = 1550$ nm and 1554 nm for $\Delta L = 100$ μm and 400 μm, respectively. The zero point of the presented wavelength detuning vector has been centered at these measured central Bragg wavelengths. As it can be seen in Fig. 3, the anticipated chirped sinusoidal spectral response has been successfully achieved and as expected, by increasing the length mismatch ΔL, the central spectral lobe shifts towards one side of the spectral response, resulting to synthesizing faster spectral modulation profile on the opposite side of the response. This translates into modifying the RF central frequency at the output of the system.

From the measured frequency responses of spectral shapers shown in Fig. 3, the optical response bandwidth and the second-order dispersion provided by the fabricated CBGs are estimated as $BW_{\text{opt}} = 1.5$ THz (~12 nm) and $\ddot{\Phi}_1 = 16.5$ ps^2, respectively. Therefore according to Eq. (11), the maximum supported TBP of the fabricated spectral shapers for generating of chirped microwave waveforms is estimated to be $TBP_{\max} \sim 233$. Recall that in this work, $|\tau| < \tau_{\min}$ to tune the sign of the RF chirp and therefore we are not exploiting this maximum TBP. From Eq. (10), $\tau_{\min}$ is ~78 ps, and the time-delay mismatch corresponding to the length mismatches of $\Delta L = 100$ μm and $\Delta L = 400$ μm in the fabricated spectral shapers are $|\tau| \sim 1.6$ ps and $|\tau| \sim 6.4$ ps, respectively. The central wavelength of the input optical pulse from the MLL has been set at the wavelength detuning values of $\delta\lambda = -4, -3, -2, 2, 3, 4$ nm. The normalized input pulse spectra extracted from the spectral response of the tunable filter in our laser system (shifted to −20dB peak power for better clarity) is also shown in Fig. 3. The generated chirped microwave waveforms are captured by a high-speed (~30 GHz) photodetector and monitored with a sampling oscilloscope (CSA8000, Tektronix Inc.) operating in sample mode.

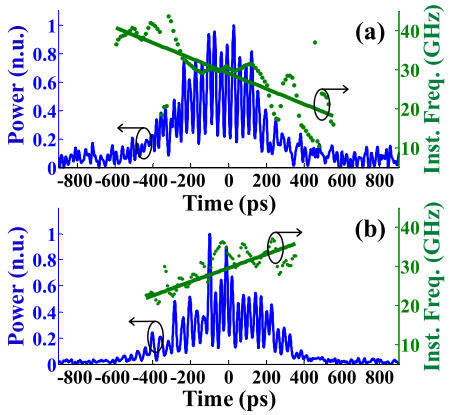

Fig. 4. The generated chirped microwave waveforms at two experimental measurement points of the curves shown in Fig. 5 with positive and negative chirp rates, i.e. for the case of spectral shaper with $\Delta L = 100\mu$m and the central wavelengths of the input optical pulse at $\delta\lambda = -4$nm (a) and $\delta\lambda = 4$nm (b). The central microwave frequency f_C and the linear chirp rate C_{RF} of theses generated microwave pulses are (a) $f_C = 29.58$ (GHz), $C_{RF} = -19.98$ (GHz/ns), and (b) $f_C = 23.76$ (GHz), $C_{RF} = +18.77$ (GHz/ns).

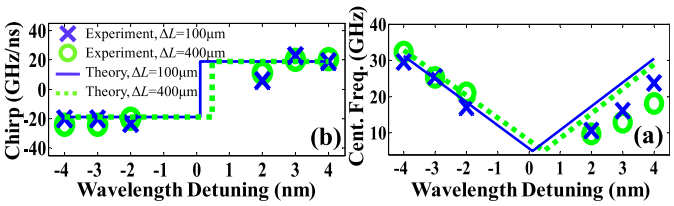

Fig. 5. Experimental measurements of the (a) central frequency (f_C) and (b) the chirp rate (C_{RF}) of generated microwave pulse waveforms versus the central wavelength of the input optical pulse.

The generated chirped microwave waveforms with positive and negative RF chirp rates for the case of the spectral shaper with $\Delta L = 100\ \mu$m and the central wavelengths of the input optical pulse at $\delta\lambda = -4$ nm and 4 nm are shown in Fig. 4. The instantaneous frequency in Fig. 4 has been extracted by using a spectrogram analysis (the dotted green curve) and then a linear curve fitting (the solid green curve). The TBP of the generated chirped microwave waveforms are approximately between 15 to 20, which is several times smaller than the TBP_{max} since the input optical pulse exploits only a fraction of the whole integrated spectral shaper response (this can be inferred from Fig. 3). Fig. 5 summarizes the measurements for the central frequency (f_C) and RF chirp rate (C_{RF}) of the generated microwave pulse waveforms versus the central wavelength of the input optical pulse. There is a fairly good agreement between the experimental measurements and the curves extracted from the above derived theoretical model, i.e., Eqs. (8) and (9). As it can be inferred from Eqs. (1-9), the imperfections of the spectral phase response of the CBG, i.e. the group delay ripples (GDRs), can cause deviations in the instantaneous frequency, and the target central frequency and chirp rate of the generated microwave pulses. This suggests improving the integrated CBG design by using some apodization techniques [15].

IV. Conclusion

We have demonstrated an integrated spectral shaper in SiP for the photonic generation of chirped microwave waveforms. In particular, we have fabricated an integrated Sagnac loop structure incorporating a CBG, which is able to provide a chirped interference spectral pattern required for generation of the chirped microwave pulses. The designed length mismatch between the arms of the fabricated Sagnac loop enables us to achieve a reconfigurable RF chirp sign along with RF central frequency tunability of the generated microwave pulse. The tunability is achieved through tuning the central wavelength of the input optical pulse. Two integrated spectral shapers with different length mismatch of the Sagnac structure have been fabricated and characterized. Moreover a simplified theoretical model for the waveform generation process based on the spectral features of the integrated CBG has been presented. The reported experimental demonstration of the integrated silicon photonic device in this work is a fundamental step towards the development of many integrated microwave photonics signal generation and processing circuits.

References

[1] D. K. Barton, *Radar System Analysis and Modeling*. Boston, MA, USA: Artech House, 2005.

[2] M. Bertero, M. Miyakawa, P. Boccacci, F. Conte, K. Orikasa, and M. Furutani, "Image restoration in chirp-pulse microwave CT (CP-MCT)," *IEEE Trans. Biomed. Eng.*, vol. 47, no. 5, pp. 690–699, May 2000.

[3] H. Kwon and B. Kang, "Linear frequency modulation of voltage-controlled oscillator using delay-line feedback," *IEEE Microw. Wireless Compon. Lett.*, vol. 15, no. 6, pp. 431–433, Jun. 2005.

[4] J. D. McKinney, D. Seo, D. E. Leaird, and A. M. Weiner, "Photonically assisted generation of arbitrary millimeter-wave and microwave electromagnetic waveforms via direct space-to-time optical pulse shaping," *J. Lightw. Technol.*, vol. 21, no. 12, pp. 3020–3028, Dec. 2003.

[5] Z. Jiang, D. E. Leaird, and A. M. Weiner, "Line-by-line pulse shaping control for optical arbitrary waveform generation," *Opt. Exp.*, vol. 13, no. 25, pp. 10431–10439, Dec. 2005.

[6] A. Zeitouny, S. Stepanov, O. Levinson, and M. Horowitz, "Optical generation of linearly chirped microwave pulses using fiber Bragg gratings," *IEEE Photon. Technol. Lett.*, vol. 17, no. 3, pp. 660–662, Mar. 2005.

[7] H. Gao, C. Lei, M. Chen, F. Xing, H. Chen, and S. Xie, "A simple photonic generation of linearly chirped microwave pulse with large time-bandwidth product and high compression ratio," *Opt. Exp.*, vol. 21, no. 20, pp. 23107–23115, Oct. 2013.

[8] J. Chou, Y. Han, and B. Jalali, "Adaptive RF-photonic arbitrary waveform generator," *IEEE Photon. Technol. Lett.*, vol. 15, no. 4, pp. 581–583, Apr. 2003.

[9] C. Wang and J. Yao, "Chirped microwave pulse generation based on optical spectral shaping and wavelength-to-time mapping using a Sagnac loop mirror incorporating a chirped fiber Bragg grating," *J. Lightw. Technol.*, vol. 27, no. 16, pp. 3336–3341, Aug. 15, 2009.

[10] R. Ashrafi, Y. Park, and J. Azaña, "Fiber-based photonic generation of high-frequency microwave pulses with reconfigurable linear chirp control," *IEEE Trans. Microw. Theory Techn.*, vol. 58, no. 11, pp. 3312–3319, Nov. 2010.

[11] M. H. Khan *et al.*, "Ultrabroad-bandwidth arbitrary radio frequency waveform generation with a silicon photonic chip-based spectral shaper," *Nature Photon.*, vol. 4, no. 2, pp. 117–122, Jan. 2010.

[12] D. Marpaung, C. Roeloffzen, R. Heideman, A. Leinse, S. Sales, and J. Capmany, "Integrated microwave photonics," *Laser Photon. Rev.*, vol. 7, no. 4, pp. 506–538, Jul. 2013.

[13] M. Burla, L. R. Cortés, M. Li, X. Wang, L. Chrostowski, and J. Azaña, "Integrated waveguide Bragg gratings for microwave photonics signal processing," *Opt. Exp.*, vol. 21, no. 21, pp. 25120–25147, Oct. 2013.

[14] J. Azaña and M. A. Muriel, "Real-time optical spectrum analysis based on the time-space duality in chirped fiber gratings," *IEEE J. Quantum Electron.*, vol. 36, no. 5, pp. 517–526, May 2000.

[15] T. Erdogan, "Fiber grating spectra," *J. Lightw. Technol.*, vol. 15, no. 8, pp. 1277–1294, Aug. 1997.